Journal Pre-proofs

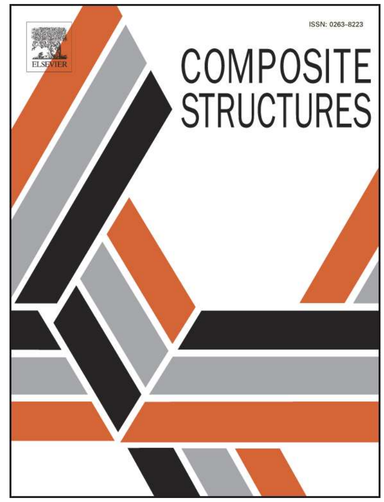

Understanding mixed mode ratio of adhesively bonded joints using genetic programming (GP)

Yiding Liu, Zewen Gu, Darren J. Hughes, Jianqiao Ye, Xiaonan Hou

PII: S0263-8223(20)33315-8
DOI: https://doi.org/10.1016/j.compstruct.2020.113389
Reference: COST 113389

To appear in: *Composite Structures*

Received Date: 1 May 2020
Revised Date: 23 September 2020
Accepted Date: 30 November 2020

Please cite this article as: Liu, Y., Gu, Z., Hughes, D.J., Ye, J., Hou, X., Understanding mixed mode ratio of adhesively bonded joints using genetic programming (GP), *Composite Structures* (2020), doi: https://doi.org/10.1016/j.compstruct.2020.113389

Understanding mixed mode ratio of adhesively bonded joints using genetic programming (GP)

Yiding Liu[a,*], Zewen Gu[b], Darren J. Hughes[a], Jianqiao Ye[b], Xiaonan Hou[b,*]

[a] WMG, University of Warwick, Coventry, CV4 7AL, UK

[b] Department of Engineering, Engineering Building, Lancaster University, Lancaster, LA1 4YW, UK

*Corresponding author's email address: yiding.liu@warwick.ac.uk; x.hou2@lancaster.ac.uk

Abstract

Adhesively bonding has been increasingly used for numerous industrial applications to meet the high demand for lightweight and safer structures. Debonding of adhesively bonded joints is a typical mixed mode failure process. It is highly depended on the interactional effects of material properties and geometric definitions of the constituents, which is very complicated. The existing studies in identifying fracture modes of joints based on either experiments or finite element analysis are often prohibitively time and computational expensive. This paper proposed an innovate method by combining Finite Element Analysis (FEA), Latin Hypercube Sampling (LHS) and Genetic Programming (GP) to understand the effect of the physical attributes on the fracture modes of adhesively single lap joints. A dataset of 150 adhesive joint samples has been generated using LHS, including different combinations of adherend and adhesive's material properties and thicknesses. The mixed mode ratios of the 150 samples are calculated using Strain Energy Release Rate (SERR) outputs embedded in Linear Elastic Fracture Mechanics (LEFM), which has been validated by experimental tests. Finally, a GP model is developed and trained to provide an extracted explicit expression used for evaluating the early-state failure modes of the adhesively bonded joints against the design variables.

Keywords: adhesively bonded joints; mixed mode ratio; finite element analysis; Latin Hypercube Sampling; Genetic Programming; Strain Energy Release Rate

1. Introduction

The adoption of multi-materials strategy has been increasingly utilised in the aerospace, vehicle and marine engineering, which facilitates the necessity of using adhesive joining technologies due to its superior characteristics, such as, high strength-to-weight ratio, excellent stress transfer behaviour and the compatibility with a wide range of material types. To ensure a safe structural assembly, it is essential to have an insight of the joint performance, of which fracture mechanism is one of the key considerations to prevent catastrophic joint failure, improve and optimise the joint design, especially when initial cracks exist. For adhesive systems where the fracture toughness of modes I and II are noticeable different, the ratio between the two modes is vitally important in choosing the appropriate failure criteria and determining the failure of the joints assembly [1]. Moreover, a better understanding of the fracture parameters and fracture mechanism of adhesively bonded joints can help design engineers with enhancing fatigue resistance and restore the stiffness and strength of the damaged/cracked structures [2].

In a practical adhesively bonded joint, debonding is a typical mixed mode fracture process, including a mixture of mode I (peel) and mode II (shear). The growth process of local or edge debonding under quasi-static or fatigue loading is usually modelled by a fracture-mechanics approach leading to the calculation of the Strain Energy Release Rates (SERRs) [3]. Campilho et al. [4] developed the fracture envelops of the Single Leg Bending (SLB) with three different adhesive types. The results show that the mixed mode energies during crack propagation are different among the different adhesives. In addition, the ratio of mode I SERR against mode II SERR (G_I/G_{II}) are also distinct among the different adhesives. Hafiz et al. [5] presented the G_I (mode I) *vs* G_{II} (mode II) for steel joints with FM73 epoxy adhesive using the closed-form Linear Elastic Fracture Mechanics (LEFM) method. It has been shown that there is a significant interaction between different failure modes and that the fracture energy of mode II is considerably higher than that of mode I. Shahin et al. [6] has proposed an asymptotic analytical model to determine the SERRs of modes I and II for balanced and unbalanced single lap joints using the edge moments and shear forces at the ends of the overlapped zone . The ratio of G_{II}/G_I in a balanced single lap joint with 3 mm thick aluminium adherends was analysed for different adhesive layer thickness by using the proposed equations and compared with the numerical results. The results show that when the adhesive layer thickness is larger than approximately 0.3 mm, the ratio of G_{II}/G_I is lower than 1 (mode I dominant), and vice versa. For the unbalanced lap joints with an initial crack, whose upper adherend was a unidirectional CFRP with fixed elastic properties and the stiffness of the lower adherend is varied from 20 GPa to

250 GPa, the ratios of mode I SERR against total SERR (G_I/G_T) were compared with the results from FE models using the Crack Tip Opening Displacement (CTOD). An increase of the modulus of the lower adherend results in a decrease in the ratio of G_I/G_T, which is reasonable as the increased stiffness makes the joint more difficult to bend. These studies have demonstrated that the fracture behaviour of the joints is significantly affected by their physical characteristics, such as materials and thicknesses. With regard to fatigue, Sahoo et al. [7] numerically evaluated the SERRs of mode I and mode II at various debonding length (from 3 mm to 5.5 mm) for adhesively bonded single lap aluminium-to-aluminium joints using Redux-39A adhesive with a pre-defined crack of 3 mm at the bond end. It was found that G_{II} was more dominating than G_I at the initial stage of crack propagation. It was also seen that the variation of G_{II} was insignificant over the disbond length, while G_I increased as debonding grew. Liu et al. [8,9] numerically studied the trends of modes I and II SERRs as the debonding grew in a composite single lap joint with a 5 mm pre-crack. It was seen that as the crack length grew from 5 mm to approximately 18 mm, both modes I and II SERRs did not vary too much and increased slowly. When the joints were close to failure, mode II SERR increased significantly due to the large bending moment effect. It can be seen that the dominant trend of G_I and G_{II} during crack propagation were altered, when different joint categories were investigated. It was concluded that the failure of adhesively bonded joints depends on several factors, such as, the materials of adherends and adhesives, initial crack length and the joint configurations (overlap length, adherend and adhesive thicknesses [10,11]), as these factors altogether have a significant collective effect on the stress distributions within the adhesive.

One of the major limitations of the current studies is that they are mainly based on one-factor-at-a-time (OFAT) technique, which only investigates the effect of one parameter rather than assessing the combined effects of a set of or all design variables on the responses of the interests. In addition, the acquirement of joints' failure scenarios is always obtained by conducting experimental tests using limited number of joint coupons, which is highly sensitive to the quality of the selected samples. It is also costly and impractical to conduct tests for every possible joint configurations. Finite Element Analysis (FEA) method is another commonly utilised method to evaluate joint behaviours. The advantages of FEA are that the boundary value problems can be resolved systematically and complex geometry can be handled [12]. However, FEA is also a time-consuming method, especially when a large number of elements and nodes is required to execute. In addition, a large number of simulations is required for a full-factorial multi-parameter analysis, which obstacles a better understanding of the interactional effects of design parameters of adhesive joints on their fracture mechanisms.

In this study, a novel approach is developed to determine the mixed mode ratio of adhesive joint. Firstly, FE models were developed to analyses the failure process of single lap adhesive joints with a pre-crack. To reduce the required amount of FE models in the parametric study, and thereby improve the computational efficiency, Design of Experiments (DoE) is applied to reduce the number of samples. The sampling technique, Latin Hypercube sampling (LHS) is also implemented. LHS was first proposed and defined by McKay et al. [13] as a type of stratified Monte Carlo sampling. Every component in this method has a fully stratified manner despite the level of its importance. The method has been widely used to construct computer experiments in problems of multidimensional distribution. Anders et al. [14] employed FE codes in conjunction with the LHS method to demonstrate its superiority over standard Monte Carlo sampling method. The same conclusion was also achieved by Olsson et al. [15], where LHS is employed to aid the structural reliability analysis. It was also found that when LHS is used in importance sampling, more than half of the computer effort could be saved comparing with the simple Monte Carlo method. A sensitivity analysis of a water-quality model was conducted by Manache and Melching [16] by applying the LHS technique, which is combined with both regression and correlation analyses. In their work, the number of design points N were taken to be four third times the number of variables to pursue satisfactory results. Recently, a paper by Liu et al. [17] utilized LHS based on Audze-Eglais criterion to generate a set of fuselage barrel design points for FE analysis. Luo et al. [18,19] applied LHS to generate 140 uniformly distributed design points for finite element modelling, the results of which were then used to optimize the structure of a piezoelectric flex transducer.

Based on the set of data attained from DoE, Genetic Programming (GP) technique was used to perform symbolic regressions for this study. The concept of GP was firstly introduced by Cramer [20], and comprehensively developed by Koza [21]. It has been widely proved in many studies [22,23] that genetic algorithms were extremely efficient in optimizing engineering structures. As an extension of genetic algorithms (GAs), GP is recently categorized as a supervised Machine Learning (ML) technique. Its solutions are usually displayed as tree diagrams that contains nodes and leafs. These diagrams can be translated into functional expressions which describe the relationships between variables. The major advantage of GP technique over traditional regression techniques lies in its robust ability of predicting objective equations without necessity of assuming their prior forms. GP technique, alongside with its variant, is therefore widely applied in engineering applications where predefined regression equations are difficult or unable to achieve. Cevik [24] sought for an explicit formulation to describe available rotation capacity of wide-flange beams using GP. Experiments on 81 specimens with a total of seven physical variables were conducted for GP model. Another paper by Cevik [25] used the same GP approach to model Reinforced Concrete (RC) beam torsional strength. 75 rectangular beams with 12 varied geometric and material properties served for achieving experimental data. Following those studies, similar studies were done by many other researchers [26–30]. In all these studies, good agreements between the model predictions and experiments were achieved. In addition, all the above works involved comparative studies between the equations generated by GP models and the empirical equations. They all results in a same conclusion that the GP approach-based model can perform much better on the prediction of material or physical properties than the traditional empirical equations.

The novelty of this work is to introduce Latin Hypercube Sampling and Genetic Programming techniques to generate and analyse 150 sets of numerical joint samples (FE models) representing different combinations of substrates and adhesives. The robustness of the FE models is validated by experimental testing using aluminium-to-aluminium identical and aluminium-to-polyphtalamide hybrid single lap joints with a 5 mm initial crack in the adhesive interface. The results show that the developed method could provide a reliable tool to obtain a good understanding of the complex early-stage failure process of all kind of single lap adhesive joints. The schematic of this paper has been illustrated in Figure 1.

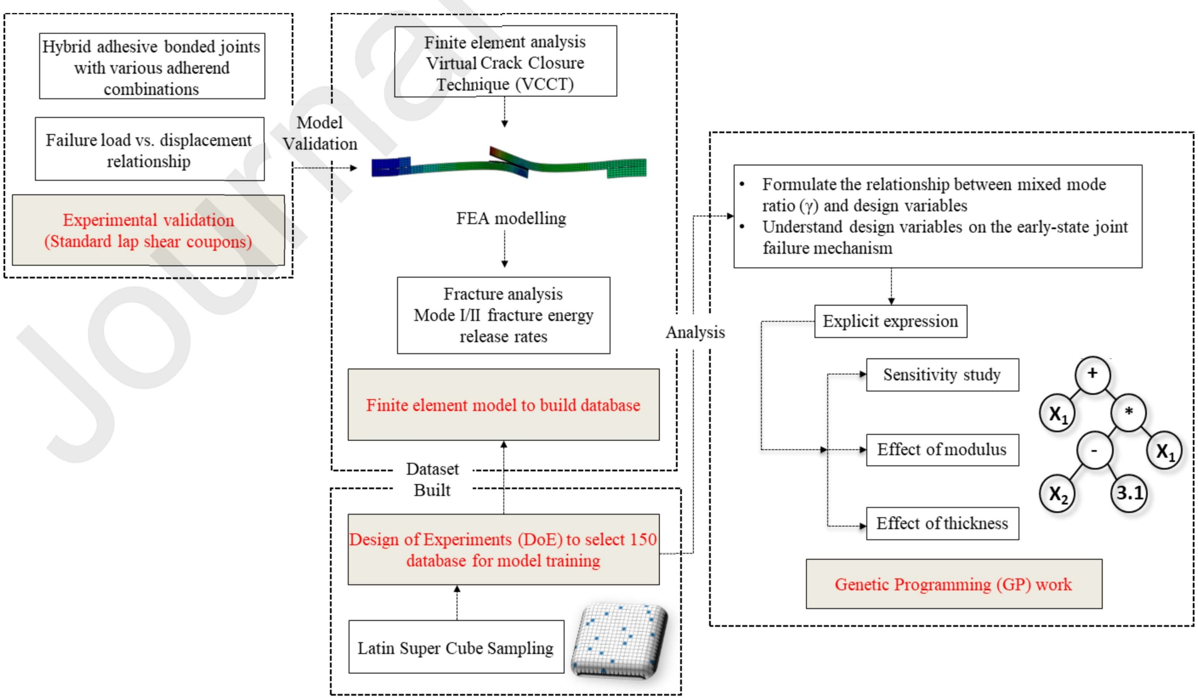

Figure 1 Schematic of joint fracture analysis based on mechanical experiments, finite element modelling, DoE and GP techniques.

2. Single lap tests

The experimental tests were conducted on two types of joints, including the identical joints using aluminium 6082 T6 and the hybrid joints consisting of both aluminium 6082 T6 and polyphtalamide (PPA) adherends. The PPA material, commercially named Grivory HTV-5H1 black 9205, is a glass fibre (50%) reinforced engineering thermoplastic material based on a semi-crystalline, partially aromatic polyamide. The geometry and dimensions of the single lap joints are adopted from ASTM D3165 standard [31], as shown in Figure 2. The width of the single lap joint is 25 mm. The adherends are bonded by Loctite EA 9497 adhesive, which is a medium viscosity, two-component epoxy adhesive. The nominal thickness of the adherend and adhesive are 3 and 0.3 mm, respectively. A thin layer of 25 μm thick Teflon release film is inserted in the middle of the adhesive to create an initial 5 mm debonding. A coupled surface treatment including the usage of grit blasting using a premium quality soda-lime glass bead (Guyson Honite Grade 12, particle size of 150-250 microns [32]) followed by cleaning with compressed air and surface cleaner (a mixture of isopropyl alcohol and distilled water in the ratio of 90:10) was carried out to improve the bonding quality. The joint specimens were cured at 120 ºC for 2 hours by using a clamping jig to ensure a uniform adhesive layer. End tabs were also bonded to reduce the bending moment and to avoid damage in the adherends during the tests. The material properties of the adherends and the adhesives were measured and are summarised in Table 1.

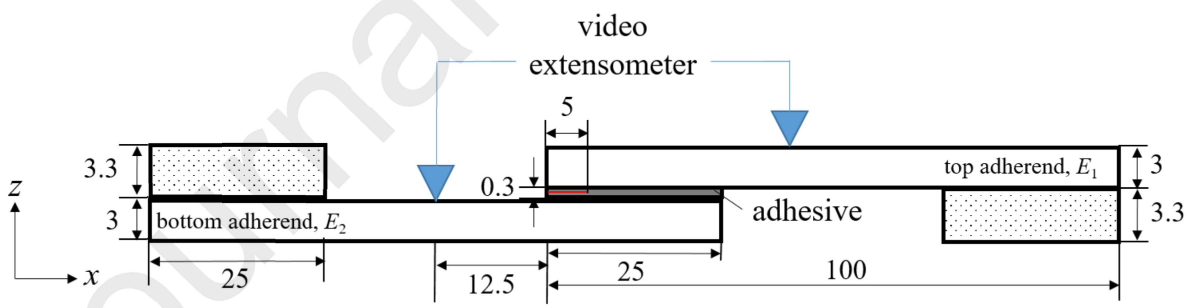

Figure 2 Geometry and dimensions of single lap joint sample with the locations for video extensometer. The width of the joints is 25 (unit: mm).

Table 1 Elastic properties of the adherends and the adhesive

	Young's Modulus (GPa)	Poisson's Ratio
Aluminium 6082 T6	70.00	0.30
Polyphtalamide (PPA)	17.62	0.32
Loctite EA 9497 adhesive	7.71	0.29

Lap shear tests of the single lap joints were carried out using an Instron 5800R machine with a 50 kN load cell, wedge-action grips and a displacement rate of 1 mm/min at room temperature. A video extensometer was used to measure the relative displacement between the two dots (measuring reference points) at a distance of 12.5 mm to the adhesive overlap, as shown in Figures 2 and 3. The experimental setup is shown in Figure 3(a). The fracture surfaces of the identical and hybrid joint samples are shown in Figure 3(b) and 3(c), respectively. The identical aluminium joints failed within adhesive (cohesive failure), with a thin layer of adhesive left on both adherends. It shows that the initial crack located at the adhesive interface has stimulated the crack propagation. However, the hybrid aluminium-PPA joint failed entirely along the interface (adhesive failure) due to the large peel stress at the overlap edge generated by the stiffness mismatch of the substrates.

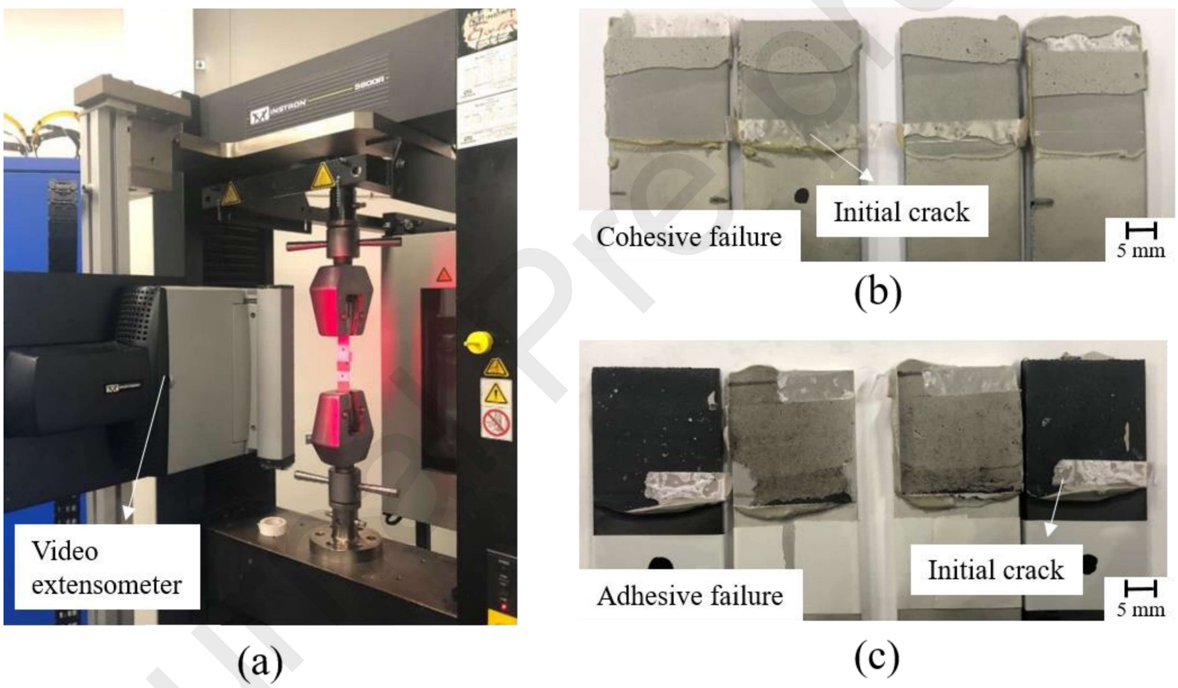

Figure 3 (a) The setup of the test machine with video extensometer, (b) the failure modes of identical Al joints and (c) hybrid Al-PPA joints.

3. Finite element analysis

The Virtual Crack Closure Technique (VCCT) is widely used to implement the delamination/debond failure criteria, which was firstly proposed by Rybicki and Kanninen [33]. This method is commonly utilized for computing Strain Energy Release Rates based on the nodal forces and displacements at the crack tip [34], primarily on the basis of Irwin's crack closure integral theory under LEFM. In a two-dimensional FE model (where G_{III} is 0), the values of G_I and G_{II} can be calculated according to Figure 4 and Equations (1)-(3). Although, the VCCT technique can only deal with the state of stress under elastic linear conditions, while J integral considers the large plastic deformation of the adhesive, it was found in [3] that the results from the finite element models with the VCCT are very close to those of J integral and show the same trend for thin epoxy adhesives. As the range of adhesive modulus discussed in this paper covers primarily epoxy adhesives which behave elastically at the initial debonding stage, the SERRs using VCCT is used in calculations.

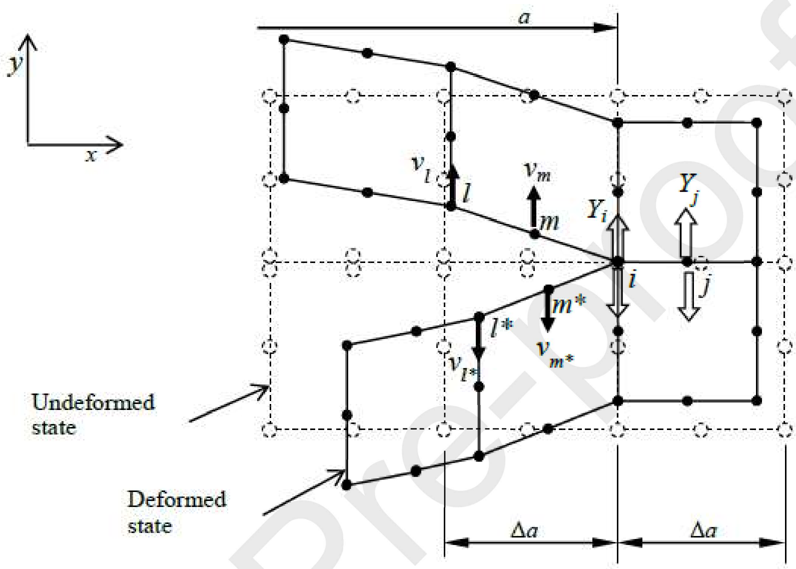

Figure 4 VCCT used in two-dimensional FE model using eight-node elements (nodal forces and displacements could be obtained from FE analysis) [33].

The SERR for mode I and mode II, G_{I} and G_{II}, are given by:

$$G_{\mathrm{I}} = \frac{-1}{2\Delta a}\left[Y_i(v_l - v_{l^*}) + Y_j(v_m - v_{m^*})\right] \tag{1}$$

$$G_{\mathrm{II}} = \frac{-1}{2\Delta a}\left[X_i(u_l - u_{l^*}) + X_j(u_m - u_{m^*})\right] \tag{2}$$

$$\gamma = \frac{G_I}{G_{II}}\ (G_{II} \neq 0) \tag{3}$$

where Δa is the length of elements around the crack tip; Y_i, Y_j, X_i, X_j are the nodal force components in the y– and x–directions at nodes i and j, respectively; v_l, v_{l^*}, v_m, v_{m^*}, u_l, u_{l^*}, u_m, u_{m^*} are the nodal displacement components in the y– and x–directions at nodes l, l^*, m, m^*, respectively [34]; γ is defined as the mixed mode ratio.

A two-dimensional FE model using VCCT technique is developed in Abaqus/CAE code 6.14 Package to predict the failure load of the joint. The FE model of lap joints employs the realistic geometries and dimensions (including the tabbed area), as shown in Figure 5. Especially, a 5 mm initial disbond is defined to simulate the one in experimental samples. Four-node plane strain elements (indicated as CPE4 elements) are used for the adherends and the adhesive. The displacements and the rotations of the entire nodes at left end are restrained in all directions whereas those at the right end are constrained against *y*-direction displacement and rotations. A displacement is applied to the right end until final failure. A mesh size of 0.25 mm is used at the bonded area after a mesh convergence study and gradual mesh size is used for the adherends to save computational time. The Benzeggagh-Kenane failure criterion [35] (Equation (4)) is considered as the debond failure criteria with fracture parameters measured from previous tests (G_{IC} = 0.22 N/mm, G_{IIC} = 0.90 N/mm measured from standard Double Cantiler Beam and End Notch Flexure tests [36]). And mixed mode ratio η of 1.75, which has been used by a number of researchers [37], is adopted in this study. Non-linear geometric analysis using explicit solver is implemented for the large deformation.

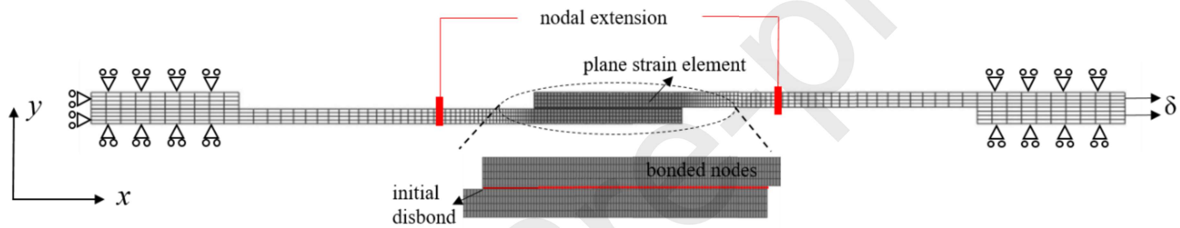

Figure 5 Load and boundary conditions of the single lap joint model.

$$\frac{G_I + G_{II}}{G_{IC} + (G_{IIC} - G_{IC})\left(\frac{G_{II}}{G_I + G_{II}}\right)^{\eta}} \geq 1 \quad (4)$$

The validation of the models is performed by comparing load *vs* extension relations with the experimental results (for three samples in each category), as shown in Figure 6. The nodal displacements taken from the FE models are compared with the extension measured from the video extensometers (as shown in Figure 2) on the experimental specimens. A good agreement has been observed by comparing the results from the experiments and the simulations for both types of joints, although the measurements from the extensometer show slight fluctuation. Besides, it can be seen that the maximum failure load is sensitive to the stiffness of adherends, dropping approximately 25% by changing one substrate from Al material (Figure 6(a)) to PPA material (Figure 6(b)). This is due to a higher peel and shear stress concentrations at the overlap edge associated to a larger bending and longitudinal deformation induced by the lower stiff adherends. The Al-PPA joint has a larger longitudinal deformation as compared to the Al-Al joint due to the stiffness difference of the adherends.

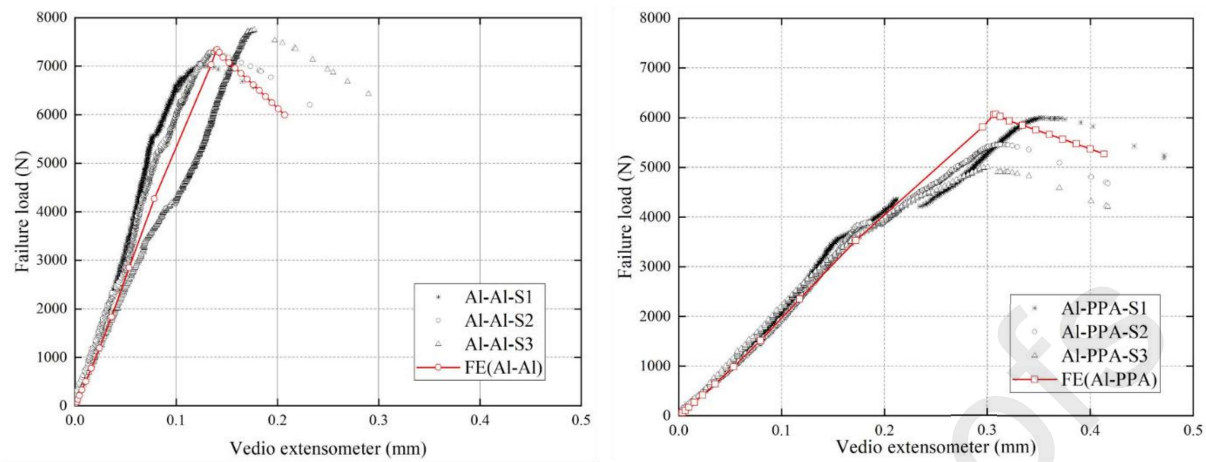

(a) (b)

Figure 6 Comparison of load vs. extensometer displacement relations from experiments and FE prediction for (a) identical aluminium joints and (b) hybrid aluminium-PPA joints.

4. Data driven models

4.1 Design of Experiments (DoE)

Using the developed FE model, a parametric study has been carried out to provide a robust database for obtaining the SERRs of mode I and mode II at the crack tips and the fracture mode ratio (γ) by using different combinations of material and thickness. The geometric design parameters of the joints are shown in Figure 7. The fixed length of the initial disbond is 5 mm. The thicknesses of the top, the bottom adherends and the adhesive are denoted as T_1, T_2 and T_a, respectively. In this study, the design space contains six parameters and they are listed in Table 2 along with their respective ranges. The ranges of the elastic modulus of the adherends (E_1 and E_2) and the adhesive (E_a) are selected from 4 to 200 GPa and 1 to 8 GPa, respectively, which cover a wide variety of adherend materials (PPA, aluminium, composites and steel) and epoxy based adhesives.

The DoE technique adopted in this work is the standard LHS. When using LHS, the number of necessary samples can be small, whilst guarantees the quality of the variable space. By employing a stratified sampling strategy, LHS assurances a uniform distribution of every samples in the design space. The main principals of the standard LHS can be considered as follows:

a. The set of the d input dimension $x = (x^1, x^2, \ldots, x^d)^T$ is divided into N equal intervals, and only one experiment is allowed in each interval.

b. When providing a dimension, k, only one sample exists in each interval and thus N scalar samples are generated.

c. By randomly matching these scalar samples in the ith dimension k_i, a N dimensional tuple $X_1, \ldots, X_N$ can be obtained.

d. To calculate the probability of the LHS by the same way of the Monte Carlo [38].

It has been recognised that LHS can usually generate samples that are more representative than those generated by conventional random sampling techniques.

150 samples are generated for this analysis by applying LHS on the six parameters. All the modelling work was based on cohesive failure that assumes a good bond between the adherends and the adhesive. A maximum displacement of 0.2 mm was applied as the external loading for all scenarios. The crack tip SERRs were then obtained to calculate the mixed mode ratio at the initial stage of the crack propagation. The mixed mode ratios (γ) of the 150 sample designs based the DoE sampling are shown in Figure 8. It can be seen that γ ranges from 0 to 7, with most of the data fall within 0 to 3 with reasonable distributions.

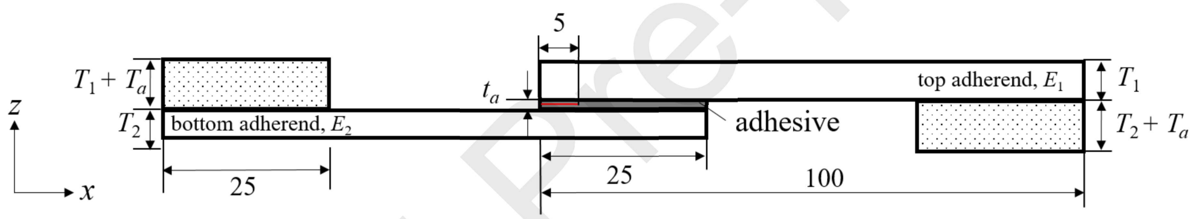

Figure 7 Geometry and dimensions of single lap joints undertook in the parametric FE studies (unit: mm).

Table 2 Six parameters considered in DoE and their lower and upper bounds

Parameters (DoE)	Lower Bound	Upper Bound
Young's Modulus of top adherend, E_1 (GPa)	4	200
Young's Modulus of bottom adherend, E_2 (GPa)	4	200
Young's Modulus of adhesive, E_a (GPa)	1	8
Thickness of top adherend, T_1 (mm)	1	8
Thickness of bottom adherend, T_2 (mm)	1	8
Thickness of adhesive, T_a (mm)	0.1	2

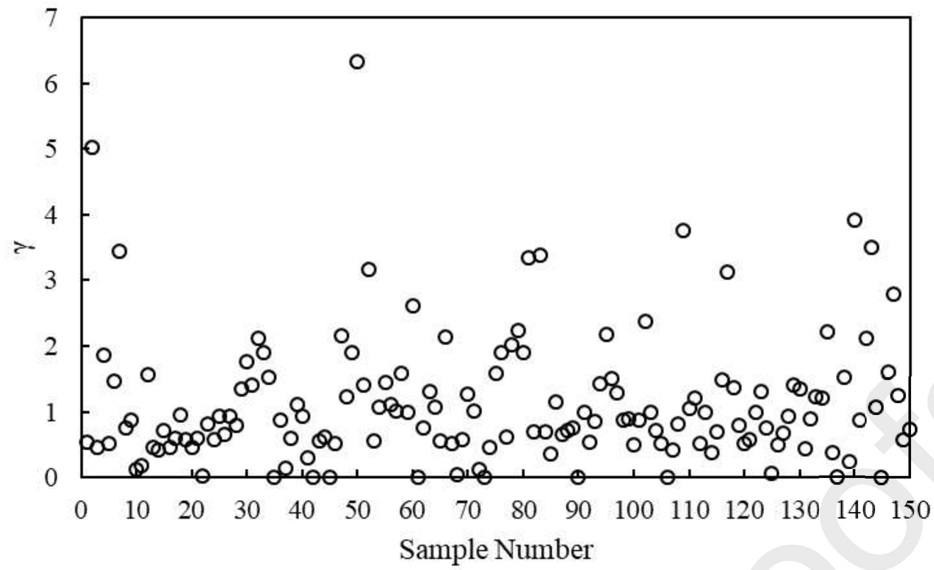

Figure 8 The fracture mode ratio γ calculated from the150 FE models. (Note: all the points close to the *x* axis have non-zero γ values)

4.2 Genetic Programming (GP)

Genetic programming (GP) is a subarea of evolutionary algorithms, which is inspired by Darwin's theory of evolution. It can be used to find the relationship among variables in the data sets. Unlike building empirical model which is usually problematic in selecting the structure of the approximation function, GP techniques is a systematic and efficient way to search for high quality global approximations. Instead of calculating the string of numbers in a GA, GP searches for the structure of computer programs that satisfies the solutions. A tree structure is normally employed to represent the expression of a program. For example, the expression $(x_1 \times x_2 - x_3)^2$ can be described as Figure 9(a). A flowchart of GP process is displayed in Figure 9(b). First, the structure of programs is initialized to allow the insertion of the parameters. Then, the evaluation of the fitness is conducted, which determines the quality of the approximations of the current generations. A poor fitness value will lead the process back to the section of tuning algorithms. The common tuning algorithms used in GP are reproduction, mutation and crossover, which perform on the connections between mathematical operators and the terminal nodes. The whole process terminates only when the value of fitness reaches an acceptable level. The final mathematical expressions determined by the tree structure program can be one of the approximation functions that is searched for.

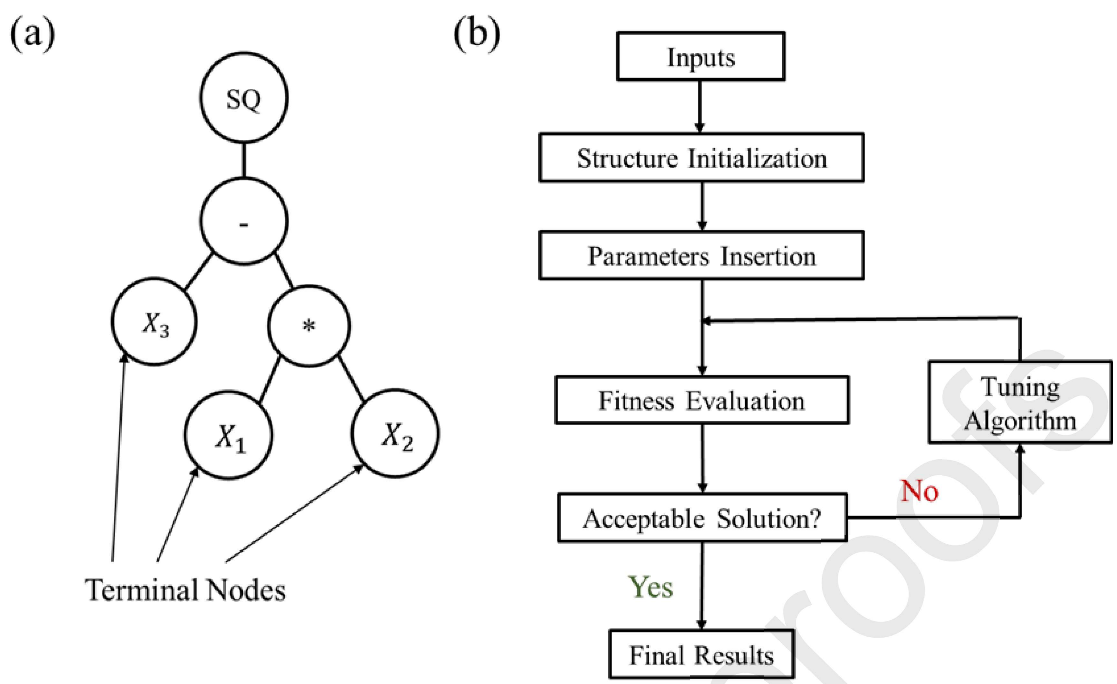

Figure 9: (a) Tree structure for the expression $(x_1 \times x_2 - x_3)^2$, (b) a brief flowchart of genetic programming process

In this paper, the GP technique is employed to formulate the relationship between the six design parameters and the mixed mode ratio (γ). The modelling of GP is implemented by using a python package 'GPlearn'. The parameters of the GP model used for regressing the current function are listed in Table 3.

Table 3 The parameters of the python programme in GPlearn

Parameters (GPlearn)	Value
Function Set	'+', '-', '*', '/'
Population Size	6000
Generations	100
Crossover	0.7
Subtree Mutation	0.1
Hoist Mutation	0.05
Point Mutation	0.1
Parsimony Coefficient	2e-4

As shown in Table 3, only linear operators are used in the function set. The fitness value is aimed to drop to below 0.20. As a result, the fitness value for the final evolutionary step is 0.198. 120 sets of samples randomly selected from the 150 sets of FE results are used for training the GP model. The remaining 30 sets of the FE results are used as the independent test sets to demonstrate the validity and effectiveness of the trained GP model.

5. Results and analysis

Firstly, an explicit expression of the trained GP model, which is based on the parameters in Table 2 and a fixed crack length of 5 mm, are generated by the developed GP algorithm, as shown in Equation (5):

$$\gamma = 0.252 E_2 T_2 \frac{2E_1 + E_2 + T_1 - \frac{E_1 T_a}{T_1} + \left(E_1 + T_1\right) T_a{}^2}{E_2 E_a T_1 + E_1 \left(T_1 + E_2 T_a\right)} \tag{5}$$

Based on the proposed Equation (5), the cross plottings of the mixed mode ratios (γ) obtained from the estimated training results (Figure 10(a)) and the predicted testing results (Figure 10(b)) against that from the FE model are presented respectively. The validation line is defined where γ from GP model is equal to the one from FE simulations. On the training phase (Figure 10(a)), the GP model is able to learn from the data samples very efficiently with high correlation coefficient and lower values of errors. It can be seen that almost 93% of the data fall into the 5% deviation range. Similarly, on the testing phase (Figure 10(b)), the high correlation achieved by the GP model suggests that the predictions obtained from the testing data are in agreement with the FE simulations. It should be noted that in the testing phase, the validation especially includes two data points for identical and hybrid joints (red and brown data point in Figure 10(b)), which was tested by experimental work. Therefore, it can be seen that the developed GP model is of a great efficiency as both the training and testing data are closely accommodated on the validation line. It should also be noted that there are only few points laying outside the area between red lines, which means good accuracies are obtained in both training and testing sets. Increasing the population size and generation could move these points into the area, however, the expense of computing time will be significant.

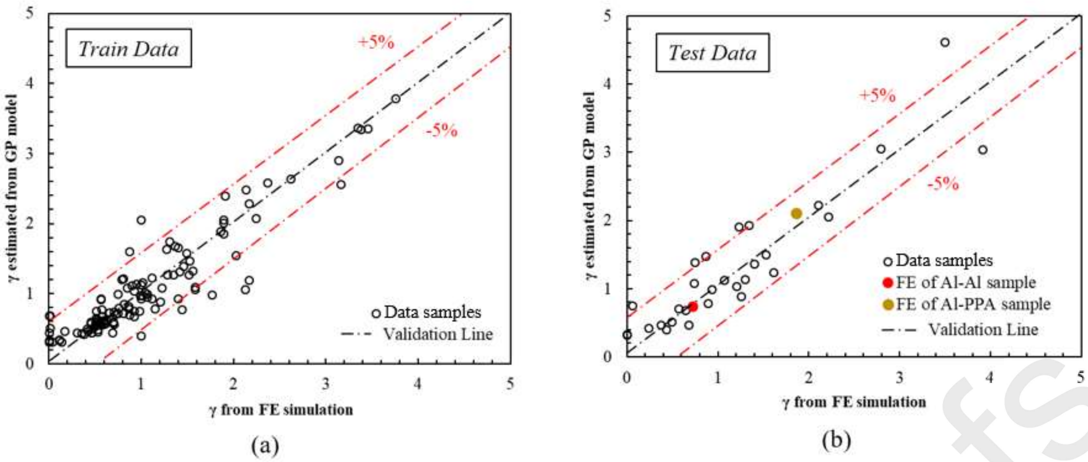

Figure 10 The correlation between GP model predicted results and FE simulated results of (a) trained data and (b) test data.

To interpret the Equation (5), a sensitivity study is conducted to analyse the impact levels of each parameter on the mixed mode ratio, γ. Sensitivity study provides an ideal method to determine the impact of each independent variable on a given set of assumptions or equations with a particular dependent variable. The model for this analysis is derived from the Python inspired package 'SALib'. The package implements a commonly used sensitivity analysis method Sobol, to calculate the effects of model inputs on outputs of interest. The argument number N applied for this study is 1000, which means 1000 values of every parameters are randomly selected from the ranges of each variables in Equation (5). The calculated sensitivities of each parameters are displayed in Figure 11. It can be seen that elastic modulus of the adherends has a much higher sensitivity than their thickness. Among all the modulus parameters, the impact of the adherend modulus is higher than the adhesive modulus (the sensitivity factor of E_2 and E_1 is 0.528 and 0.156 compared to 0.01 for E_a). Among the parameters of thickness, the thickness of adhesive (T_a) has higher (0.058) impact on the mixed mode ratio than other two T_1 (0.001) and T_2 (0.032).

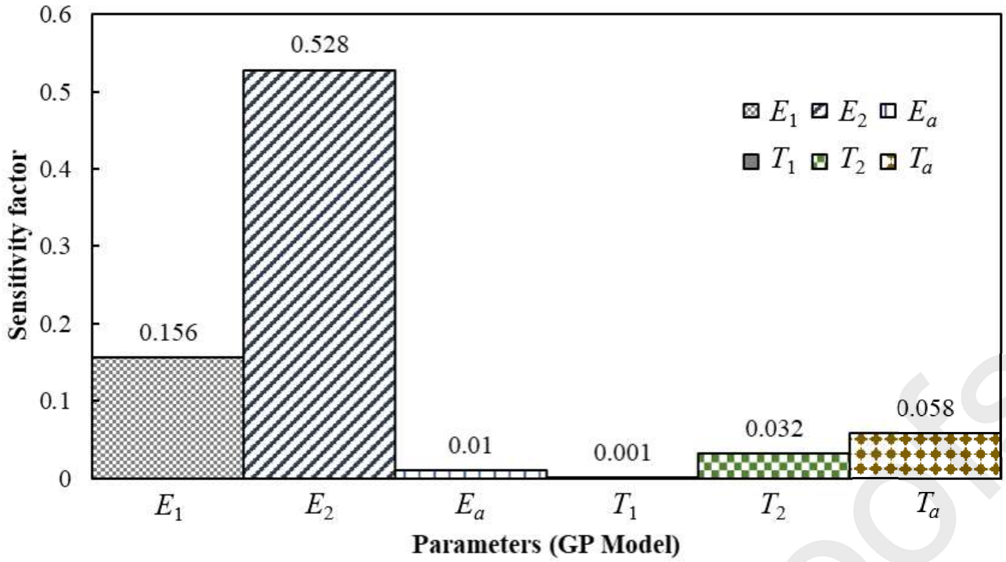

Figure 11 The sensitivity study on the design parameters of the joint on the mixed mode ratio based on developed GP model.

5.1 Effect of modulus

In this sensitivity study, all the results are obtained only by using the Equation (5), which avoids the lengthy calculations by using FE method. According to the results, the material properties of the constituents of the joint determinedly affect the character of the stress distribution at the crack tip, and therefore alternate the failure modes of the joints. Consequently, the effect of modulus is evaluated separately with fixed thicknesses for the adherends ($T_1 = T_2 = 3$ mm), and the adhesive (T_a = 0.3 mm) corresponded to the geometry of the real experimental samples. The same Python package, 'SALib', is used to produce 5000 sets of data points randomly. In these sets, the elastic modulus (E_1, E_2 and E_a) are variables within the same ranges in Table 2, whilst the thickness (T_1, T_2 and T_a) are constants. The values of mixed mode ratio γ, corresponding to the 5000 sets of data are obtained by substituting these values into Equation (5). The main relationship of the mixed mode ratio, γ against E_a and E_1/E_2 is shown in Figure 12(a). When E_a is constant at 7.71 GPa (Loctite EA 9497 adhesive), the relationship of γ against E_1/E_2 is ploted in Figure 12(b). It is interesting to find that the mixed mode ratio increases with the increase of E_1/E_2. When E_1/E_2 is smaller than 1.56, γ (G_I/G_{II}) is lower than 1. It indicates that mode II is dominant during the failure process. When E_1/E_2 is higher than 1.56, γ is higher than 1. It indicates that mode I is dominant during the failure process. This is true as a large difference between the elastic moduli of two adherends could generate a large rotation and bending on the comparatively weaker adherend, thus resulting in high peel stress at the crack tip and further fracture failure. This behaviour has also been approved by Sawa et al. [39] who analysed the stress distributions within dissimilar single lap adheisve joints using the two-dimensional theory of elasticity. It was found that at the edge of overlap of a epoxy adhesive joint, the peel stress (σ_y) is almost constant with the increase of E_1/E_2, whilst, the magnitude of the shear stress (τ_{xy}) reduced significantly [39]. This also indicated model I is the dominante mode of failure.

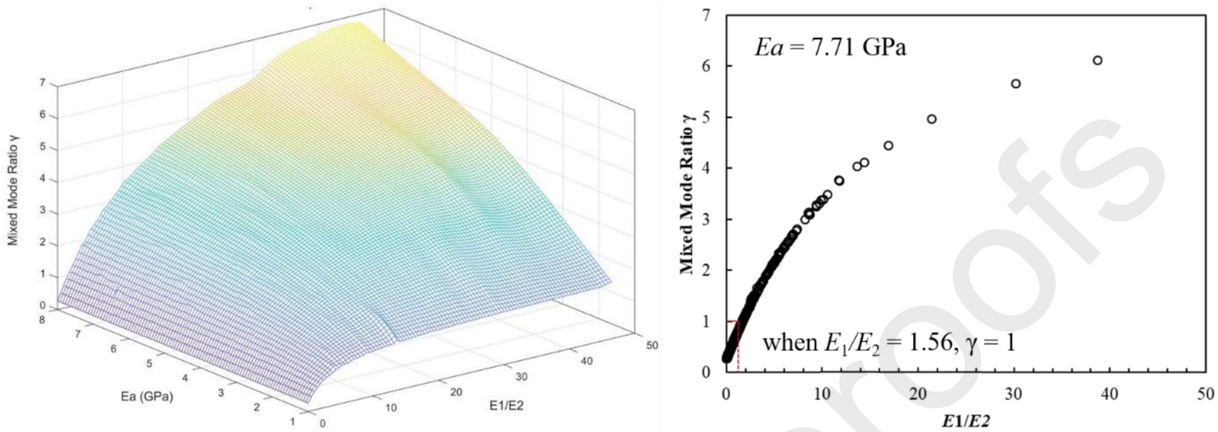

(a) (b)

Figure 12 The relationship between mixed mode ratio γ and material properties of the constituents, when $T_1 = T_2 = 3$ mm and $T_a = 0.3$ mm: (a) γ against E_a and E_1/E_2, (b) γ against E_1/E_2 when E_a=7.71 GPa.

5.2 Effect of thickness

Although the sensitive level of the thickness of the constituents on the mixed mode ratio γ is lower than that of their material properties, it is still necessary to understand it when the materials of constituents are determined. The evaluation of the thickness effect has been conducted on identical (Al-Al) and hybrid (Al-PPA) joints with Loctite adhesive (the properties are shown in Table 1) respectively, as shown in Figure 13. For the identical joint, γ increases with the increase of T_a, when T_1 and T_2 are constants (3 mm). When T_a is smaller than 1.38 mm, γ is lower than 1. It means that the joint is mode II dominant. When the adhesive is thicker than 1.38 mm, γ is higher than 1, the joint tends to be dominated by mode I failure. This can be explained by that when the adhesive is thin, the peel and shear stresses are affected substantially by the adherend stiffness. The peel stress will increase as the thickness of the adhesive increases [39] and a considerable bending stress will occur at the interfaces as the adhesive becomes thicker. It is also found that the thickness of individual adherend does not have a determinative effect on the mixed mode ratio γ, when the thicknesses of the other adherend and the adhesive are fixed as shown in Figure 13(b) and 13(c). According to these figures, it can be conclude that for identical joint, the failure model is mainly dominated by G_{II} (γ smaller than 1), except when the thickness of adhesive is relatively large.

For the hybrid joint, when T_1 and T_2 are constants (3 mm), γ reduces slightly when T_a is smaller than 0.5 mm (Figure 13(d)). When T_a exceeds 0.5 mm, a rapid increase of γ is observed. This is due to that the stress in the adhesive is affected by the combination of the longitudinal and the bending deformations of the PPA material. For all the hybrid joints, however, γ is higher than 1, which means that G_I is always the dominate mode of failure. This may be attributed to that the mode of fracture of the hybrid joints is primarily determined by their mechanical properties of the constituents, thus alternations of the thickness, which is a less sensitive parameter, do not alter the overall mode of failure, as shown in Figure 13(d)-(f).

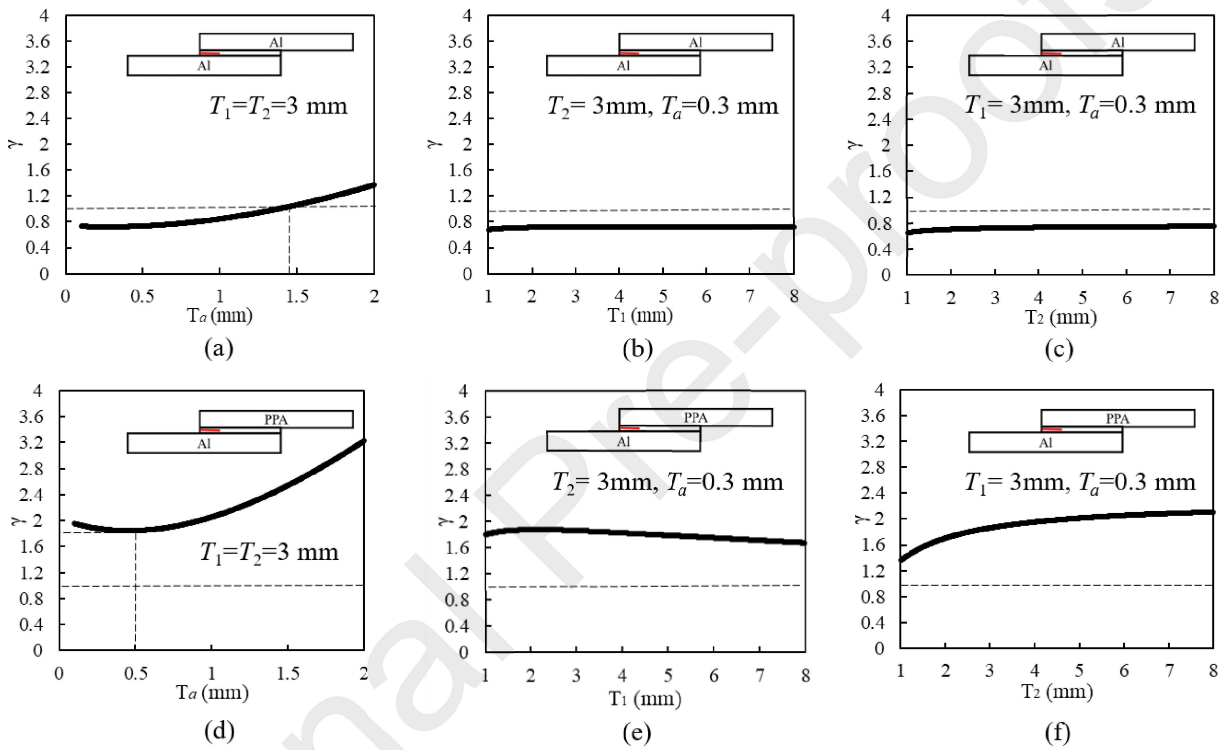

Figure 13 The relationship of mixed mode ratio, γ against T_a, T_1 and T_2 of Al-Al joints (a)-(c), and PPA-AL hybrid joints (d)-(f).

The effects of T_2/T_a on the mixed mode ratio γ of identical joints (Figure 14(a)) and hybrid joints (Figure 14(b)) are examined, respectively. T_1 is fixed to 3 mm since its sensitivity factor is only 0.001, due to the location of the initial disbond (Figure 11). According to the results, there is no simple evident relationship between γ and T_2/T_a. It seems that the fracture mode is more determined by the absolute magnitudes of the thicknesses rather than the ratio of T_2/T_a. For instance, for the identical joints, when the T_2/T_a is smaller than 6.87, one T_2/T_a value could correspond to different values of γ, which could be either higher than 1 or lower than 1. It depends on the individual value of the thickness, as it has a noteworthy effect on the stress distribution within the joint. However, when the value of T_2/T_a is larger than 6.87, the joint is consistently mode II dominant (γ < 1). This can be explained that if T_a is significantly thin compared to T_2, then the bending moment can be negligible, leading to the adhesive deformed primarily in shear loading. With the further increase of the value of T_2/T_a, the mixed mode ratio γ approaches a constant at approximate 0.8. For the hybrid joints, all the joints fail in mode I, regardless of the magnitudes of T_2/T_a (Figure 14(b)). It shows that the failure mode of hybrid joint is mainly determined by the material properties of the constituents as discussed in the previous sections. In addition, γ tends to be a constant at approximately 2.1 as T_2/T_a increases.

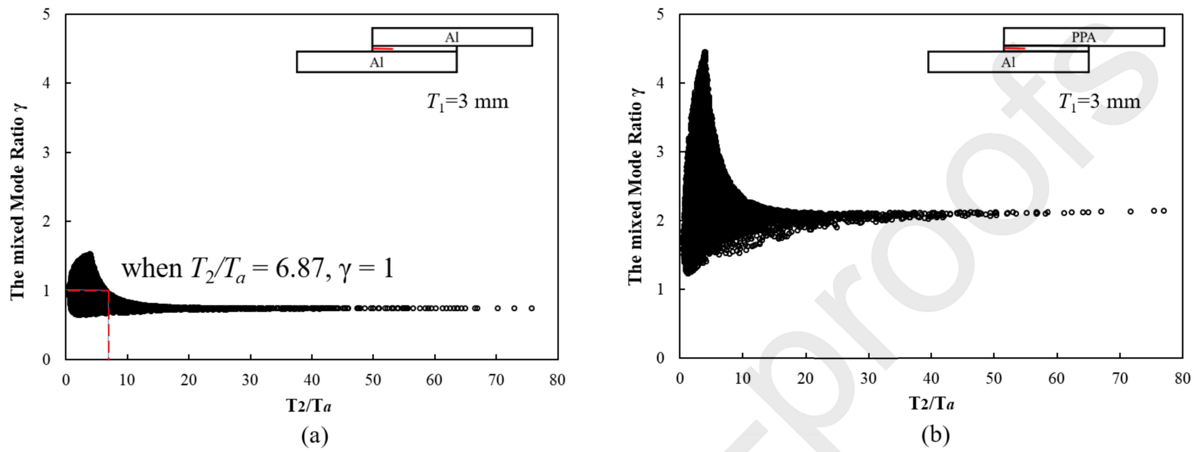

Figure 14 Effects of the T_2/T_a on the mixed mode ratio γ of the (a) identical joints (Al-Al) and (b) hybrid joints (Al-PPA), respectively with a fixed T_1 of 3 mm.

6. Conclusion

This paper presents an novel study, combining Finite Element Analysis (FEA), Latin Hypercube Sampling (LHS) and Genetic Programming (GP) to understand the effects of the physical attributes (including material properties and thicknesses of the constituents) on the early-state fracture modes of adhesively single lap joints (with an initial disbond of 5 mm in the adhesive). A number of 150 numerical joint samples with different combinations of substrates and adhesives has been developed based on the analysis of LHS. The validation of the FE models has been carried out using the experimental results. The crack tip Strain Energy Release Rates (SERRs) were obtained using Virtual Crack Closure Technique (VCCT) assuming that both the adherends and the adhesive are under elastic deformation and at the initial stage of the crack propagation. The GP model, which was trained and tested using the data generated based on the FE models, has been applied to analyse the effect of different physical parameters on the fracture modes of the joints. The obtained results have demonstrated that the developed analysis strategy provide an effective and robust method to understand the mixed mode failure of adhesive joints.

The following conclusions can be withdrawn based on the above study:

- The trained GP model can predict the failure mode of adhesive joints with a good agreement with the FEA simulations as well as experimental tests. The extracted explicit expression (Equation (5)), which describes the relationship among the mixed mode ratio (γ), the material and thickness of the joint constituents has been proposed and validated. It could be applied in analysing the effect of any variable on the failure mode of adhesive joints made of a wide variety of adherend materials (aluminium, composites and steel) and most of epoxy adhesives. Although, the developed expression is limited for analysing the early-state fracture as the SERRs are obtained based on a 5 mm initial crack, it is still significant in guiding design and optimization in practice.
- The material properties of substrates (E_1 and E_2) has a determinative effect on the joint's fracture mode. When the magnitude of E_a is fixed, a one-to-one correspondent relationship can be summarized between the mixed mode ratio γ and E_1/E_2. For instance, when E_1/E_2 is smaller than 1.56 (for fixed E_a of 7.71 GPa), γ is smaller than 1, which indicates mode II dominant failure and vise versa.
- The effect of thickness of constituent is minor comparing with the effect of material properties on the mixed mode ratio, γ. However, when the materials of substrates are fixed, the effect of adhesive thickness (T_a) is more significant compared to adherend thicknesses (T_1 and T_2), which could determine the failure mode of the joint. For the identical joint (Al-Al joints with initial disbond), the failure model is mainly dominated by mode II failure (γ smaller than 1), the only exception is the case when the thickness of adhesive (T_a) is relatively large. For the hybrid joint (Al-PPA joints with initial disbond), mode I failure dominates in all the cases as γ always larger than 1.

References:

[1] Camanho PP, Davila CG, Pinho SS. Fracture analysis of composite co-cured structural joints using decohesion elements. Fatigue Fract Eng Mater Struct 2004;27:745–57.

[2] Mehrabadi F. Experimental and numerical failure analysis of adhesive composite joints. Int J Aerosp Eng 2012;2012:1–10.

[3] Chadegani A, Yang C, Dan-Jumbo E. Strain-energy release rate analysis of adhesive-bonded composite joints with prescribed interlaminar crack. J. Aircr., vol. 46, 2009, p. 203–15.

[4] Santos MAS, Campilho RDSG. Mixed-mode fracture analysis of composite bonded joints considering adhesives of different ductility. Int J Fract 2017;207:55–71.

[5] Hafiz TA, Abdel Wahab MM, Crocombe AD, Smith PA. Mixed-mode fracture of adhesively bonded metallic joints under quasi-static loading. Eng Fract Mech 2010;77:3434–45.

[6] Shahin K, Taheri F. The strain energy release rates in adhesively bonded balanced and unbalanced specimens and lap joints. Int J Solids Struct 2008;45:6284–300.

[7] Sahoo PK, Dattaguru B, Manjunatha CM, Murthy CRL. Fatigue de-bond growth in adhesively bonded single lap joints. Sadhana - Acad Proc Eng Sci 2012;37:79–88.

[8] Liu Y, Lemanski S, Zhang X, Ayre D, Yazdani H. A finite element study of fatigue crack propagation in single lap bonded joints with process-induced disbond. Int J Adhes Adhes 2018; 87: 1–18.

[9] Liu Y, Zhang X, Lemanski S, Nezhad HY, Ayre D. Experimental and numerical study of process-induced defects and their effect on fatigue debonding in composite joints. Int J Fatigue 2019;125:47–57.

[10] Han X, Jin Y, da Silva LFM, Costa M, Wu C. On the effect of adhesive thickness on mode I fracture energy - an experimental and modelling study using a trapezoidal cohesive zone model. J Adhes 2020;96:490–514.

[11] Li W, Guo S, Giannopoulos IK, He S, Liu Y. Strength enhancement of bonded composite laminate joints reinforced by composite Pins. Compos Struct 2020;236:111916.

[12] Capuano G, Rimoli JJ. Smart finite elements: A novel machine learning application. Comput Methods Appl Mech Eng 2019;345:363–81.

[13] McKay MD, Beckman RJ, Conover WJ. A comparison of three methods for selecting values of input variables in the analysis of output from a computer code. Technometrics 2000;42:55–61.

[14] Olsson AMJ, Sandberg GE. Latin hypercube sampling for stochastic finite element analysis. J Eng Mech 2002;128:121–5.

[15] Olsson AMJ, Sandberg G, Dahlblom O. On Latin hypercube sampling for structural reliability analysis. Struct Saf 2003;25:47–68.

[16] Manache G, Melching CS. Sensitivity analysis of a water-quality model using latin hypercube sampling. J Water Resour Plan Manag 2004;130:232–42.

[17] Liu D, Zhou X, Toropov V. Metamodels for Composite Lattice Fuselage Design. Int J Mater Mech Manuf 2015;4:175–8.

[18] Luo L, Liu D, Zhu M, Ye J. Metamodel-assisted design optimization of piezoelectric flex transducer for maximal bio-kinetic energy conversion. J Intell Mater Syst Struct 2017;28:2528–38.

[19] Luo L, Liu D, Zhu M, Liu Y, Ye J. Maximum energy conversion from human motion using piezoelectric flex transducer: A multi-level surrogate modeling strategy. J Intell Mater Syst Struct 2018;29:3097–107.

[20] Cramer NL. A representation for the Adaptive Generation of Simple Sequential

Programs. Int. Conf. Genet. Algorithms Appl., 1985, p. 183–7.
[21] Koza JR. Genetic programming as a means for programming computers by natural selection. Stat Comput 1994;4:87–112.
[22] Daraji AH, Hale JM, Ye J. New Methodology for Optimal Placement of Piezoelectric Sensor/Actuator Pairs for Active Vibration Control of Flexible Structures. J Vib Acoust Trans ASME 2018;140.
[23] Daraji AH, Hale JM, Ye J. Active Vibration Control of a Doubly Curved Composite Shell Stiffened by Beams Bonded with Discrete Macro Fiber Composite Sensor/Actuator Pairs. J Dyn Syst Meas Control Trans ASME 2018;140.
[24] Cevik A. Genetic programming based formulation of rotation capacity of wide flange beams. J Constr Steel Res 2007;63:884–93.
[25] Cevik A, Arslan MH, Köroğlu MA. Genetic-programming-based modeling of RC beam torsional strength. KSCE J Civ Eng 2010;14:371–84.
[26] Beiki M, Bashari A, Majdi A. Genetic programming approach for estimating the deformation modulus of rock mass using sensitivity analysis by neural network. Int J Rock Mech Min Sci 2010;47:1091–103.
[27] Tanyildizi H, Çevik A. Modeling mechanical performance of lightweight concrete containing silica fume exposed to high temperature using genetic programming. Constr Build Mater 2010;24:2612–8.
[28] Assimi H, Jamali A, Nariman-zadeh N. Sizing and topology optimization of truss structures using genetic programming. Swarm Evol Comput 2017;37:90–103.
[29] Al-Mosawe A, Kalfat R, Al-Mahaidi R. Strength of Cfrp-steel double strap joints under impact loads using genetic programming. Compos Struct 2017;160:1205–11.
[30] Tsai HC, Liao MC. Modeling Torsional Strength of Reinforced Concrete Beams using Genetic Programming Polynomials with Building Codes. KSCE J Civ Eng 2019;23:3464–75.
[31] ASTM D3165. Strength properties of adhesives in shear by tension loading of single-lap-joint laminated assemblies. vol. 07. 2014.
[32] Guyson International Limited. Blast media data sheet-Guyson Honite. 2019.
[33] Rybicki E, Kanninen M. A finite element calculation of stress intensity factors by a modified crack closure integral. Eng Fract Mech 1977;9:931–8.
[34] Krueger R. Virtual crack closure technique: History, approach, and applications. Appl Mech Rev 2004;57:109.
[35] Kenane M, Benzeggagh M. Mixed-mode delamination fracture toughness of unidirectional glass/epoxy composites under fatigue loading. Compos Sci Technol 1997;57:597–605.
[36] Kanani AY, Liu Y, Hughes DJ, Ye J, Hou X. Fracture mechanisms of hybrid adhesive bonded joints: Effects of the stiffness of constituents. Int J Adhes Adhes 2020;102:102649.
[37] Shindo Y, Shinohe D, Kumagai S, Horiguchi K. Analysis and Testing of Mixed-Mode Interlaminar Fracture Behavior of Glass-Cloth⁄Epoxy Laminates at Cryogenic Temperatures. J Eng Mater Technol 2005;127:468.
[38] Morio J, Balesdent M. Estimation of rare event probabilities in complex aerospace and other systems: A practical approach. Elsevier Inc.; 2015.
[39] Sawa T, Liu J, Nakano K, Tanaka J. A two-dimensional stress analysis of single-lap adhesive joints of dissimilar adherends subjected to tensile loads. J Adhes Sci Technol 2000;14:43–66.